Towards a Universal Model of Dielectric Breakdown

Andrea Padovani
Engineering Department "Enzo Ferrari" (DIEF) | University of Modena and Reggio Emilia
Via P. Vivarelli 10, 41125 Modena (MO), Italy - andrea.padovani@unimore.it

Paolo La Torraca
Department of Sciences and Methods for Engineering (DISMI) | University of Modena and Reggio Emilia
Via G. Amendola 2, 42122 Reggio Emilia (RE), Italy - paolo.latorraca@unimore.it

Jack Strand and Alexander Shluger
Department of Physics and Astronomy | University of College London
Gower Street, London WC1E 6BT, UK - jack.strand.14@ucl.ac.uk; a.shluger@ucl.ac.uk
(Jack Strand is also with Applied Materials-MDLx Italy, Reggio Emilia, and with Nanolayers Research Computing Ltd., London, UK)

Valerio Milo and Luca Larcher
MDLx Italy | Applied Materials
Via Meuccio Ruini 74/L, 42124 Reggio Emilia (RE), Italy – valerio_milo@amat.com; luca_larcher@amat.com

***Abstract*— We present a microscopic breakdown (BD) model in which chemical bonds are weakened by carrier injection and trapping into pre-existing structural defects (precursors) and by the electric field. The model goes much beyond the existing ones by consistently explaining the role of both current (a weakness of the E model) and temperature (a weakness of the power-law model), along with the role of the electric field. It also explains the non-Arrhenius temperature dependence of BD. It suggests a new comprehensive physics-based framework (with tight connections to material properties) reconciling the many breakdown theories proposed so far (E, power-law, 1/E, …) within a more universal breakdown model.**

***Index Terms*-- Dielectric Breakdown, Ginestra®, bond-breakage, precursors, carriers' injection.**

I. Introduction

Gate dielectrics breakdown (BD) is one of the most challenging areas in the field of semiconductor device reliability. Despite massive research efforts conducted for over 50 years by industry and academia, a consensus has not yet been reached on the microscopic nature of the degradation process leading to BD, and none of the models proposed over the years, such as [1]-[4], provides a comprehensive and consistent description of all the experimental observations. Also, the adoption of new materials [5] and 3D geometries (FinFET, GAA, Nanosheet) [6] complicates the scenario. Furthermore, time-dependent dielectric breakdown (TDDB) testing is typically done under field- and/or temperature-accelerated conditions. Reliable models are thus required to interpret the results and extrapolate them to real operating conditions. Having an accurate, physics-based breakdown model is thus vital for a correct prediction of device lifetime (or, equivalently, of the maximum operating voltage for 10 years lifetime).

Among the variety of the proposed models, the ones based on thermochemical (TC) bond-breakage [7]-[9], 1/E [10], [11] and power-law (PL) [12], [13] are the most relevant and widely adopted. The first relies on a physics-based description of the bond breakage process [7] and is connected to the microscopic structure and properties of the material, while the PL implements a more empirical/phenomenological approach. When applied to experimental data of accelerated TDDB tests as in Fig.1, the models give quite different lifetime extrapolations. In particular, the thermochemical model is too conservative and results in overly stringent design limitations. For this reason, it is typically disregarded by industry in favor of the power-law model (and, less often, of the 1/E model, that is overly relaxed) that provides larger design margins (that is, a higher maximum operating voltage, Fig. 1).

An obvious question, that is still a subject of heated discussions in the reliability community, is whether the use of such an empirical model is valid and really advantageous. For example, it does not provide predictive capabilities, since it must be applied on real device data every time a change is made to process and/or technology. Nevertheless, experimental TDDB data performed at low-voltage and long stress times have shown evidence of a power-law dependence of the time to breakdown on the electric field and stress voltage [14], [15]. On the other hand, the thermochemical model, which has much more solid physics foundations connected to the material microstructure [7], also predicts many of the experimental observations [4].

In this paper, we present a model that reconciles different theories (thermochemical, power law, 1/E,…) within a unique physics-based framework, consistently explaining key TDDB experimental trends. The model stems from recent results highlighting the critical role of carriers' trapping into pre-existing defects (precursors) [16]-[19] in facilitating the bond

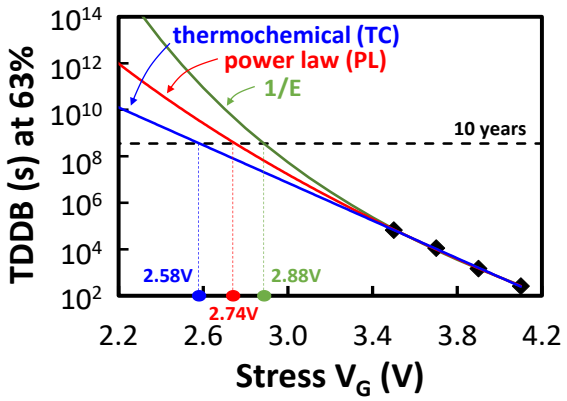

Figure 1. Best fit of experimental TDDB data (corresponding to a failure rate of 63%) collected on nFET devices with a 2.9nm-thick SiO_2 gate dielectric, obtained with (blue) thermochemical, (red) power-law, and (green) 1/E breakdown models. Experimental data (symbols) are taken from [41].

breaking process leading to dielectric degradation and breakdown. Using a commercial device simulation software [20] that implements the new physical mechanisms, we demonstrate that the TDDB E-dependence (typical of the thermochemical model) that is observed at high stress voltages (used for accelerated test conditions) evolves into a power-law dependence at moderate/low stress voltages. This change originates from the voltage/field dependence of charge carrier trapping at precursors sites, a prerequisite for the weakening and subsequent breaking of materials' bonds. The proposed model is successfully applied to reproduce TDDB data measured on SiO_2 and HfO_2 dielectrics.

II. The Carrier Injection (CI) Breakdown Model

The developed breakdown model comprises three key material-dependent processes, shown in Fig. 2 for the case of the SiO_2: (i) the presence of precursor electron trapping sites, such as oxygen vacancies (VO) and specific structural features in amorphous oxides, like wide O-Si-O bond in SiO_2 [16], [18], [21] or elongated bonds in HfO_2 [19], [22], capable of trapping two electrons; (ii) the breakage of the adjacent bond, weakened by electron trapping at the precursor site, electric field and temperature [Fig. 2 (steps 1-3), and Fig. 3]; and (iii) an effective process leading to the formation of new precursors that provides the self-sustainability to the whole mechanism (steps 4-5 in Fig. 2).

A. *Density Functional Theory Calculations*

These processes (Figs. 2 and 3) have been investigated in amorphous SiO_2 by combining classical molecular dynamics (MD) calculations of amorphous structures with Density Functional Theory (DFT) calculations of precursor trap properties [16] as well as energy barriers [21] and field acceleration factors for the trap generation processes [18]. Similar mechanisms have been demonstrated also in both crystalline [23] and amorphous HfO_2 [19], [22] and are being investigated in other materials (e.g. Al_2O_3, TiO_2, Ga_2O_3, HZO), suggesting their possible universality. DFT calculations [24] suggest the wide O-Si-O bonds and the elongated Hf-O bonds as the fundamental VO precursors in SiO_2 and HfO_2, respectively. Electron trapping by VO facilitates creation of new VOs nearby both in SiO_2 and HfO_2 [see for example Fig.

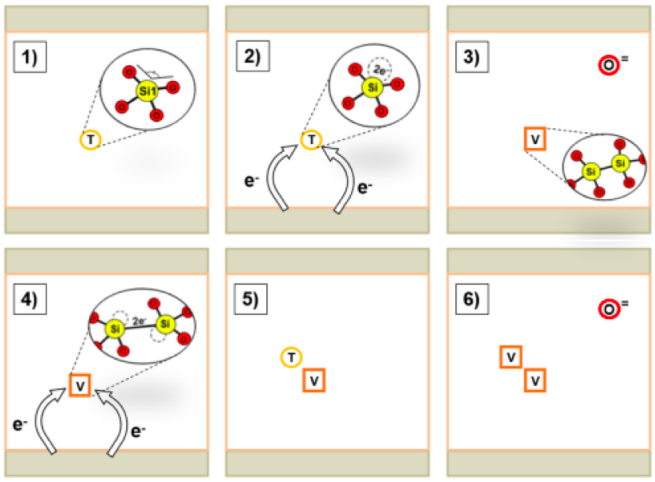

Figure 2. Schematic representation of the two-electron injection-driven microscopic processes at the bases of the degradation and breakdown. 1) Precursor (T) in SiO_2. 2) Two electrons occupy precursor. 3) Field- and temperature-activated oxygen vacancy (V) generation. 4) Two electrons occupy a vacancy. 5) Generation of a new precursor. 6) Field- and temperature-activated generation of a second vacancy (after two electrons are trapped into the precursor).

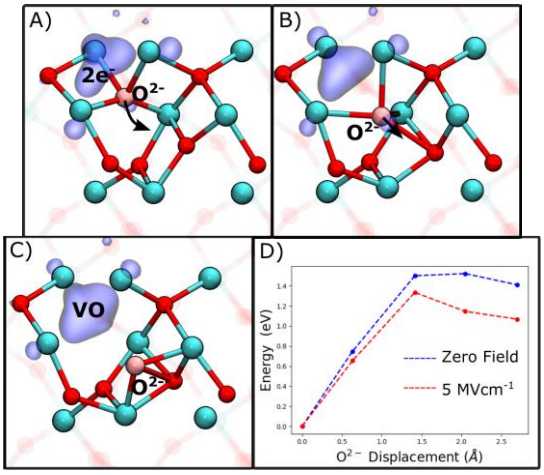

Figure 3. Schematic representation of the two-electron injection-driven vacancy formation in HfO_2. A) HfO_2 precursor defect occupied by two electrons. B) Oxygen ion displaced due to thermal fluctuation. C) Interstitial-Vacancy pair formed. D) Energy profile of the defect formation, indicating the effect of energy reduction under field stress.

2 (steps 5 and 6)] [17], [24]. This so-called "energetic correlation" effect, where pre-existing O vacancies locally increase the generation rate of additional vacancies, accelerates the oxide degradation process [19]. The dynamics of such processes is, however, material dependent [24]: in SiO_2 a doubly occupied VO can generate a new wide O-Si-O bond which in turns could generate a new VO, while in HfO_2 new VO can be directly generated from a doubly occupied VO, acting as a VO precursor itself. The described carrier-assisted processes provide an explanation of the VO formation, despite the strength of the involved bonds. DFT calculations [25] demonstrate that an applied electric field only weakly affects barriers for the creation of oxygen vacancy-interstitial defect pairs and diffusion of interstitial O ions in monoclinic HfO_2. The results demonstrate that, even close to breakdown fields, barriers for defect pair generation

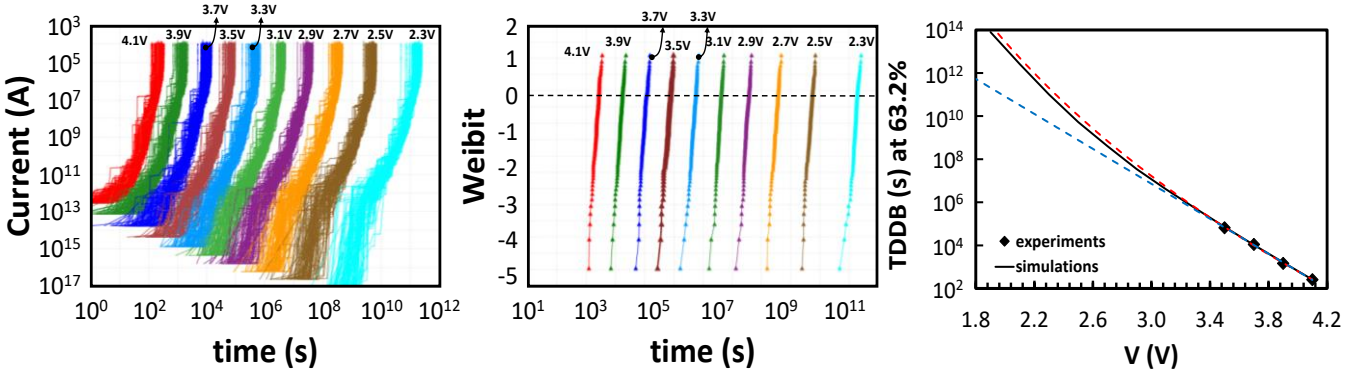

Figure 4. Results of statistical TDDB simulations performed on a Si/SiO2(29Å)/TiN stack with stress voltages between 2.3V and 4.1V. (a) Current-time characteristics. (b) TDDB Weibull plots. (c) 63.2% TDDB versus the stress voltage as extracted from (b). Results obtained with (blue dashed line) classical thermochemical equation and (red dashed line) power law extrapolation are also shown for comparison. 100 randomly generated devices are considered for every stress condition. Experimental data (symbols) are taken from [41].

exceed 6 eV in the perfect m-HfO_2 lattice. However, injection of extra electrons from electrodes significantly lowers barriers for defect creation (Fig. 3D), which are further reduced by the field to around 1 eV. Thus, bias application facilitates the injection of electrons into the oxide; these extra electrons reduce energy barriers for the creation of O vacancies, and these barriers as well as those for O ion diffusion are further lowered by the field.

B. *Ginestra® Device Simulations*

The proposed model has been implemented in the Ginestra® simulation software [20], a multi-scale defect-centric simulation platform [17], [26]-[29]. Ginestra simulations self-consistently account for the electrostatics, the charge trapping/emission processes to/from atomic defects, and the charge transport through the material stack by different conduction mechanisms. Direct/Fowler-Nordheim tunneling, drift and thermionic emission are considered consistently with trap-assisted tunneling (TAT), which controls the conduction in a wide variety of materials [26], [30]-[32]. TAT is described in the framework of the multi-phonon theory accounting for carrier-phonon coupling and lattice relaxation processes, [26], [33]-[36]. Defects are treated as discrete entities characterized by thermal ionization (E_T) and relaxation energies (E_{REL}), that depend on their atomistic structures and are calculated using DFT [19]. Local power dissipation and temperature increase associated with the charge transport, distortion and breakage of atomic bonds promoted by field, temperature and electron injection, diffusion of atomic species, are also self-consistently included, thus enabling the modeling of material modifications associated to the electrical stress and specific material properties. Calculations are performed considering the potential given by the applied bias and the defect charge state and occupation.

The rate of VO generation is modeled with the effective energy description of the bond breakage [8], [37], [38], that we modified to account for the bond weakening determined by carriers' injection and trapping:

$$G = G_0 f_{2e}\, exp\left(-\frac{E_A - p_0 \frac{2+k}{3} F}{k_B T}\right) \quad (1)$$

G_0 is the bond vibration frequency, $E_{A,2e}$ the energy required (in absence of electric field) to break the bond when two electrons are trapped at the precursor site, p_0 is the bond polarizability (describing how much the bond is distorted by the applied electric field), k the material dielectric permittivity, and k_B the Boltzmann's constant. The classical thermochemical/effective energy formulation has been modified by introducing the probability for the precursor site to be occupied by two electrons, f_{2e}. This term accounts for the carrier injection-driven degradation processes (Fig. 3) and allows reconciling the different BD theories within the same physics-based model. f_{2e} is calculated by solving the charge continuity equation at trap sites, while accounting for all the possible incoming (trapping) and outgoing (emission) transfer rates (trap-to-traps, trap-to-bands, trap-to-electrodes), determined within the multi-phonon theory:

$$R_C = N(E) f(E) P_T(E) Ca \quad (2)$$
$$R_E = N(E)[1 - f(E)] f(E) P_T(E) Em \quad (3)$$

$N(E)$ and $f(E)$ are the (energy dependent) density of states and Fermi-Dirac occupation probability, respectively; P_T is the (energy dependent) electron tunneling probability, calculated using the Wentzel–Kramers–Brillouin (WKB) approximation; Ca and Em are the multi-phonon capture and emission rates [17], [26], directly linked to the precursor ionization and relaxation energies reported in Table I.

The rate of precursors generation (steps 4-5 in Fig. 2) is modeled with equations similar to (1)-(3), while considering the precursors properties reported in Table I.

III. Results and Discussion

Figure 4 shows the results of statistical TDDB simulations performed on a MOScap device with a 29 Å-thick SiO_2 dielectric for a wide stress voltage (V_G) range (2.3V-4.1V) while considering the carrier injection-driven degradation process discussed in Section II. The simulated current-time (I-t) traces are shown in Fig. 4(a). As expected, higher initial current and faster timescale are obtained as the stress voltage is increased from 2.3V to 4.1V. More importantly, the same behavior is observed regardless of the applied V_G: the current gradually increases as oxygen vacancies are generated (by

Precursor Property	SiO_2	HfO_2 [19]	Description
$E_{T,D(Q-1)}$ (eV)	1.5	1	first electron capture
$E_{T,D(Q-2)}$ (eV)	1.5	1.1	second electron capture
ΔE_T (eV)	0.5	0.8	
$E_{REL,D(Q-1)}$ (eV)	1.5±0.3	1±0.3	first electron capture
$E_{REL,D(Q-2)}$ (eV)	1±0.4	1.1±0.3	second electron capture
Generation by Precursor	SiO_2	HfO_2 [19]	Description
$E_{A,2e}$ (eV)	0.7±0.4	1.7±0.3	SiO_2: wide O-Si-O bond → VO
p_0 (eÅ)	4	1	HfO_2: elongated Hf-O bond → VO
Generation by VO	SiO_2	HfO_2 [19]	Description
$E_{A,2e}$ (eV)	1.2	1.3	SiO_2: VO → VO + wide O-Si-O bond
p_0 (eÅ)	5	1	HfO_2: VO → 2VO

TABLE I. Parameters of the microscopic mechanisms considered in the developed breakdown model. D(Q), D(Q-1) and D(Q-2) are the charge state of the trap when empty, after single electron trapping and after double electron trapping, respectively. E_T and E_{REL} are traps' thermal ionization and relaxation energies, respectively. $E_{A2,e}$ and p_0 are the activation energy and bond polarizability of the generation process, respectively, see Eq. (1).

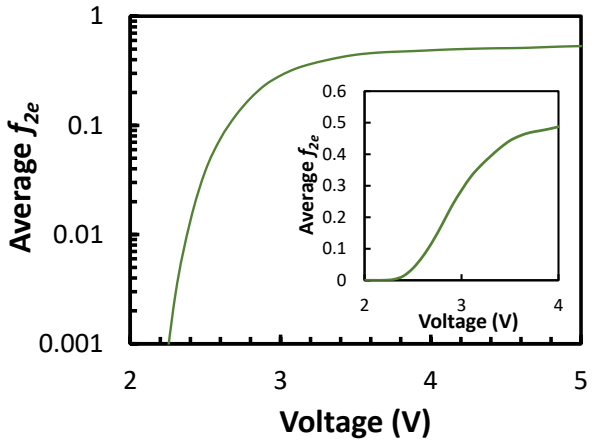

Figure 5. Average precursors' $2e^-$ occupation probability f_{2e} obtained by averaging the values of 1000 discrete precursors randomly generated within the simulated 100x100nm^2 SiO_2 device as in Fig. 4. For V_G < 2.4V, the average f_{2e} shows an exponential dependence on V_G, although it has very small values (only a small fraction of the precursors is occupied by two electrons and can therefore promote the breaking of the Si-O bonds, ~1% at V_G = 2.4V). For V_G > 2.4V, the average f_{2e} increases linearly with the voltage and then saturates to ~0.5 at V_G = 3.6V (around 50% of the 1000 precursors present in the device are filled by two electrons and can contribute to the Si-O bond-breakage process). Saturation occurs at a value lower than 1 determined by the dynamics of the electron capture/emission processes at precursor sites. Simulations show that in the considered device most of the precursors close to the gate electrode are not able to retain the trapped electrons and thus remain in their initial D(Q) state, since electrons emission (toward the gate) is much faster than their capture (R_C << R_E).

means of the carrier injection driven O-Si-O to VO conversion process, steps 1-3 in Fig. 2) until the formation of a dominant defect cluster triggers the thermal runaway phase that quickly leads to the breakdown [17], [37], corresponding to the steep current jumps in Fig. 4(a). The corresponding TDDB Weibull plots are shown in Fig. 4(b). While the Weibull slope is preserved regardless of V_G, an increasing time dependence is observed at the lower stress voltages. When the 63.2% TDDB is extracted and plotted versus the stress voltage in Fig. 4(c), a clear deviation from the trend of the pure thermochemical model emerges at low V_Gs, unveiling a power-law dependence. This is a direct consequence of the electron injection contribution captured by f_{2e} in (1), which provides a voltage-dependent modulation of the oxygen vacancy generation rate associated to the voltage-dependent probability of the precursors to capture two electrons, which is reported in

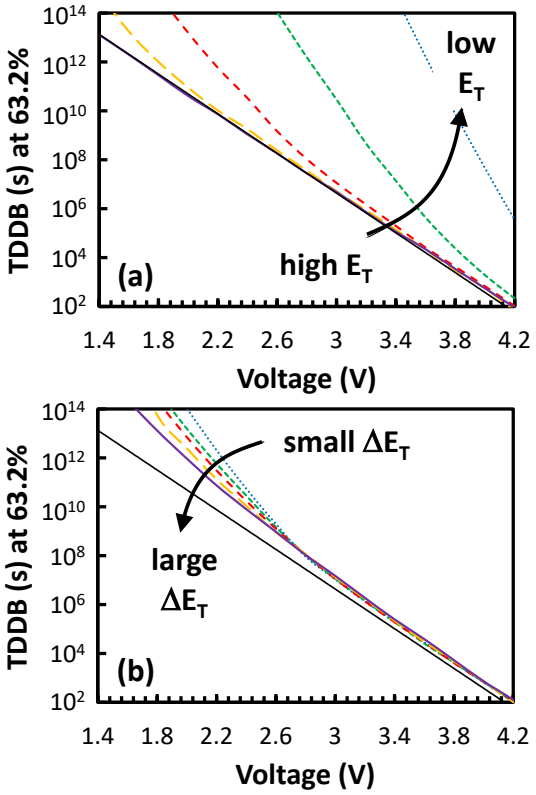

Figure 6. TDDB vs V_G plots simulated as a function of precursors' (a) E_T, and (b) E_T spread, ΔE_T, considering the proposed CI BD model. The solid black line indicates the E-dependence.

Fig. 5. When the stress voltage is equal or higher than 3.6V (corresponding to the stress conditions typically considered in accelerated TDDB tests), precursors occupation reaches an equilibrium, with most of them in the two electrons [D(Q-2)] state. Consequently, f_{2e} becomes almost constant, as shown in Fig. 5 (with a value depending on stack thickness and composition) and Eq. (1) results in the classical thermochemical model (with the E_A and p_0 values reported in Table I for the O-Si-O + $2e^- \rightarrow$ VO process). As a result, the simulated 63.2% TDDBs aligns on the E-dependence represented by the dashed blue line in Fig. 4(c). For stress voltages below 3.6V, f_{2e} reduces significantly, which determines a reduction of the oxygen vacancy generation rate, Eq. (1), and thus an increase of the breakdown time. This eventually determines a deviation of the TDDB vs. V_G plot from the E-dependence. Since the f_{2e} reduction is larger as V_G is smaller (Fig. 5), also this deviation becomes larger at lower stress voltages, resulting in the power-law dependence obtained in the 63.2% TDDB simulations shown in Fig. 4(c), that well reproduce the power-law extrapolation from the experimental TDDB data (red dashed line).

The role of electron trapping precursors is crucial for explaining and interpreting the different experimental TDDB vs. V_G trends. It is the type of precursor defect (tightly connected to material properties and process conditions) that determines, through its thermal ionization and relaxation energy properties, the shape of the 63.2% TDDB vs. V_G plot, as well as whether, how and at what voltage a deviation from the E-dependence occurs.

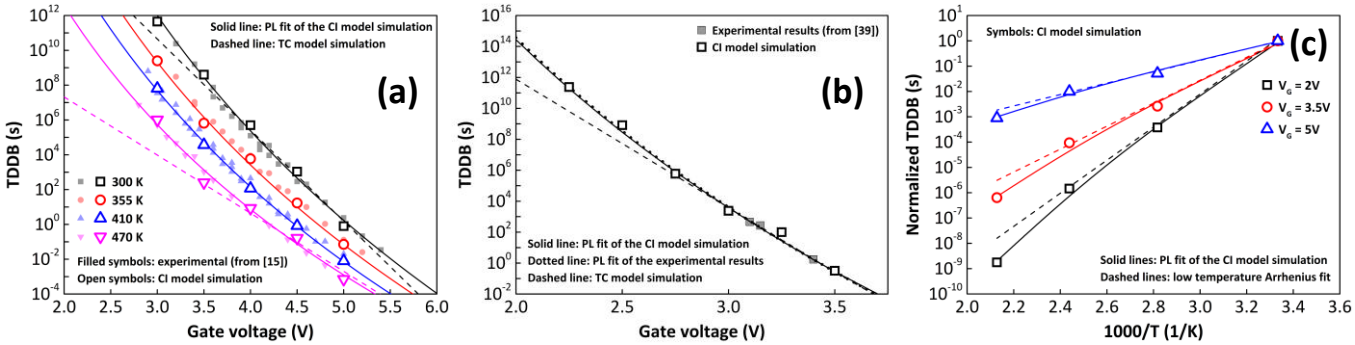

Figure 7. 63.2% TDDB data (open symbols) simulated and (filled symbols) measured (a) as a function of the temperature on nMOS capacitors with a 2.67nm-thick SiO_2 (data from [15]), and (b) on a 5nm-thick HfO_2 MIM (data from [39]). Dashed lines represent the TDDB vs V_G characteristics obtained considering a plain thermochemical model that is, with $f_{2e} = 1$ in Eq. (1). (c) Same simulated TDDB data as in (a) plotted versus the inverse of the temperature in a typical Arrhenius plot. The adoption of the CI model leads to the previously observed non-Arrhenius behavior [40].

To better investigate this aspect, we performed additional TDDB simulations and obtained the TDDB vs. V_G plot as a function of precursors' properties. Results are shown in Fig. 6 for variations of precursors' average thermal ionization energy E_T and thermal ionization energy spread (ΔE_T). As can be seen, the presence of either an *E*-dependence, a PL-dependence, or other voltage dependencies is connected to precursors' E_T and ΔE_T, Fig. 6(a)-(b). These findings have important implications for the explanation of the many – and sometimes contradicting – experimental TDDB vs. V_G trends reported in the literature. In fact, the proposed carrier injection BD model not only reconciles TC and PL theories within a unique physics-based framework, but also provides a theoretical description that can explain why the BD, even for the same material, can exhibit different voltage dependencies (as for example in the case of the SiO_2, that has been shown to follow both *E*-dependence [7] and PL-dependence [15]). Results in Fig. 6 clearly show that the presence of either a E/TC or a PL dependence of the TDDB on V_G is connected to precursors' properties, which depends not only on the material *per se*, but also on the process conditions (that may lead to different precursors even within the same material).

The CI BD model has been used to reproduce experimental TDDB data measured on SiO_2-based MOSFETs [15] and HfO_2-based MIM capacitors [39]. Figure 7(a) shows a comparison between TDDB simulations and experiments performed as a function of the temperature on nMOS capacitors with a 2.67nm-thick SiO_2 dielectric [15]. Results clearly show that a plain TC model (dashed lines) cannot explain neither the temperature dependence (unless considering different bond-breakage parameters for each temperature), nor the voltage dependence of the experimental data (especially the small bending shown at low V_Gs). Conversely, the model based on carrier injection well describes the power-law nature of the TDDB data for all the considered stress temperatures, while considering a unique set of parameters consistent with the ones reported in Table I and in a previous work [17].

Similar results are obtained also for the case of a HfO_2 film, Fig. 7(b), for which a similar process of bond weakening induced by carrier injection and trapping into pre-existing defects has been recently demonstrated [18], [19], [22], [23]. Although the limited set of available experimental data does not show any evidence of a power-law voltage dependence (being limited to the high-voltage region), simulations performed with the proposed model correctly reproduce the power-law extrapolation (dotted line). Parameters of HfO_2 precursors (elongated Hf-O bonds) and VO generation processes considered in simulations have been derived by DFT calculations [19] and are reported in Table I.

The CI model also allows to reproduce some key experimental TDDB trends, such as the non-Arrhenius temperature dependence reported for SiO_2 [40], Fig. 7(c). Simulations show that this behavior originates from the different temperature dependencies of the two concurrent processes that lead to the BD: the double electron capture into the precursors and the breakage of the weakened bond.

The Ginestra® device simulation platform implementing the CI BD model allows to investigate and understand in detail the dynamics of the VO generation process. To this end, the evolution of precursors and oxygen vacancies distribution (along the thickness and in the X, Y plane), the occupation probability of precursors' state D(Q-2) in the X, Y plane, and the current driven by traps (both precursors and VO) in the X, Y plane, are shown in Figs. 8 and 9 as obtained from the simulation of the 2.67nm-thick SiO_2 in Fig. 7(a) at 300K for two of the stress voltages considered, respectively 3V and 5V. In both cases, simulations start with precursor defects uniformly distributed within the simulated device volume [cyan spheres in Fig.8(a) and 9(a) – only the 10x10 nm^2 region in proximity of the BD spot is shown]. Upon the application of the stress voltage, carriers start flowing through the oxide and interact with existing traps. Double electron trapping into precursors promotes the breakage of Si-O bonds, leading to the formation of an oxygen vacancy [process depicted in Fig. 2, steps 1-3]. Double electron trapping into generated vacancies has a 50% of probability to induce the formation of an additional precursor [process depicted in Fig. 2, steps 4-6]. Note that this second process can happen only once for each VO, being related to the local lattice distortion induced by the vacancy.

Simulation results show that the evolution of the degradation is similar independently on the stress voltage. (timing is of course different, as shown in Fig. 4 and as discussed below). The generation of the initial oxygen vacancies brings the device in the so-called Stress-Induced

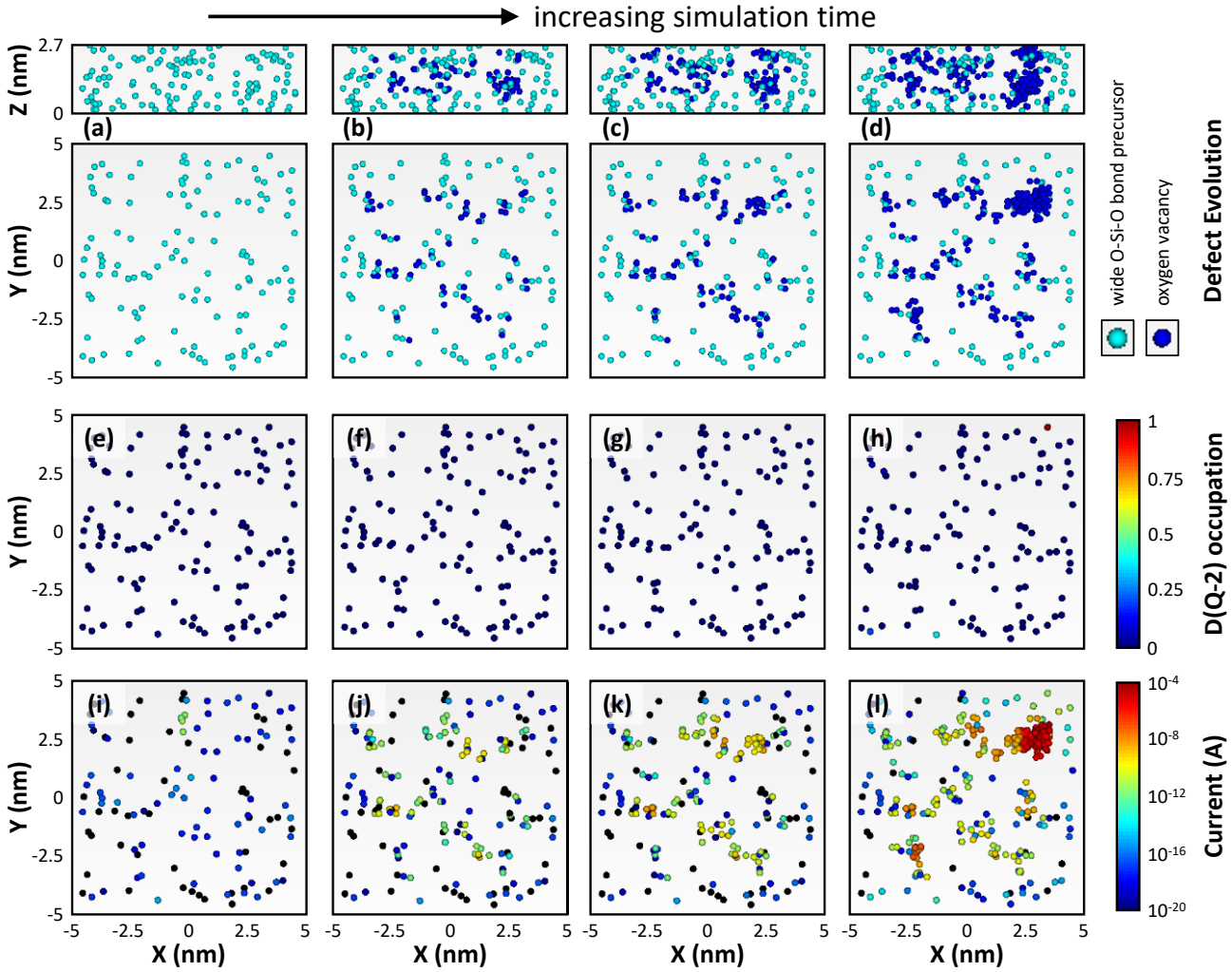

Figure 8. Evolution of (from top to bottom): (a)-(d) distribution of precursors and oxygen vacancies along the thickness and in the X, Y plane (cyan and blue spheres represent wide O-Si-O bond precursors and oxygen vacancies, respectively); (e)-(h) 2D (X, Y) map of the occupation probability of precursors' D(Q-2) state that is, the local f_{2e}; (i)-(l) 2D (X, Y) map of the current driven by precursors and VO traps. All maps are shown for subsequent phases of the degradation process (from left to right: fresh device, SILC, SBD/PBD, and HBD) as simulated at 300K with a stress voltage of 3V.

Leakage Current (SILC) stage, characterized by uniform degradation, Figs. 8(b) and 9(b), and current distribution, Fig. 8(j) and 9(j). It is also important to notice that the current is driven primarily by oxygen vacancies as evident from the comparison of the 2D maps of defects and current in Figs. 8 and 9, with the highest current points closely corresponding to the VO distribution. As more and more vacancies are generated, the device enters the soft/progressive BD stage (SBD/PBD), characterized by the formation of one or more spots with a higher local concentration of vacancies, Figs. 8(c) and 9(c), that sustain a larger current with respect to the rest of the device, Figs. 8(k) and 9(k). The corresponding increase of the local power dissipation and temperature triggers a thermally driven positive feedback that eventually leads to the thermal runaway phase and hard breakdown, characterized by the formation of a dominant BD spot, Figs. 8(d) and 9(d), that drives most of the current, Figs. 8(l) and 9(l). This spot is typically the evolution of one of those generated during the PBD phase. Finally, it is important to underline that the process is further facilitated by the parallel generation of additional precursors (mechanism in Fig. 2, steps 4-6), without which it would be self-limited and would end as soon as all precursors have been converted into vacancies.

Although they share the same evolution, the degradation of oxides stressed at different voltages is characterized by rather different time scales, since the mechanisms controlling the VO generation process – electron injection and trapping into precursors – strongly depend on the applied voltage. This can be appreciated by comparing the occupation probability of precursors' D(Q-2) state during the stress performed at 3V, see Figs. 8(e)-(h), and 5V, see Figs. 9(e)-(h). When the stress is performed at low voltages, almost all precursors are characterized by a very small occupation probability (consistent with the average f_{2e} in Fig. 5), which determines a strong reduction of the pre-exponential term $G_0 f_{2e}$ in (1) and thus a large deviation from the E-dependence in the TDDB vs. V_G plot, as seen in Fig. 7(a). On the contrary, at the high stress voltage of 5V, a significant portion of the wide O-Si-O bond traps is occupied by two electrons, see red spheres in Figs. 9(e)-(h). Therefore, since throughout the duration of the stress it is always possible to find multiple Si-O bonds weakened by

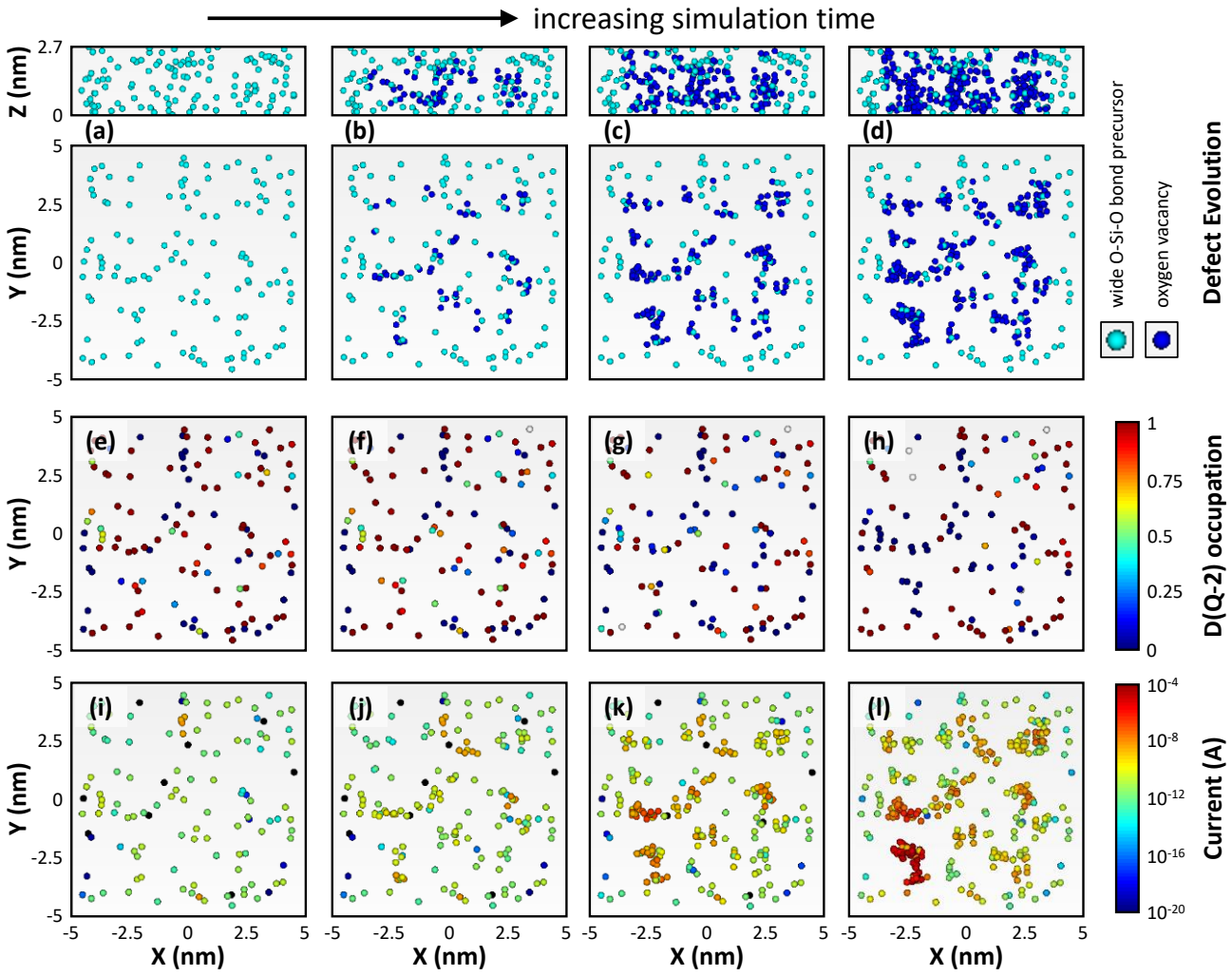

Figure 9. Evolution of (from top to bottom): (a)-(d) distribution of precursors and oxygen vacancies along the thickness and in the X, Y plane (cyan and blue spheres represent wide O-Si-O bond precursors and oxygen vacancies, respectively); (e)-(h) 2D (X, Y) map of the occupation probability of precursors' D(Q-2) state that is, the local f_{2e}; (i)-(l) 2D (X, Y) map of the current driven by precursors and VO traps. All maps are shown for subsequent phases of the degradation process (from left to right: fresh device, SILC, SBD/PBD, and HBD) as simulated at 300K with a stress voltage of 5V.

the double electron trapping into adjacent precursors, the term f_{2e} is constant and Eq. (1) takes the form of the classical thermochemical model. The bond-breakage process is very efficient and the TDDB vs. V_G plot follows the E-dependence, see for example Fig. 7(a).

IV. Conclusions

We presented a new microscopic, material-related BD model that reconciles the many breakdown theories proposed so far (E, power-law, 1/E, …) within a universal model. The model explains the transition from the *E*- to the *power law*-dependence of the TDDB on the stress voltage and correctly reproduces its temperature and field dependencies in different materials.

References

[1] J. H. Stathis, "Percolation models for gate oxide breakdown," Journal of Applied Physics 86, p. 5757, 1999. DOI: https://doi.org/10.1063/1.371590.

[2] R. Degraeve, B. Kaczer, and G. Groeseneken, "Degradation and breakdown in thin oxide layers: mechanisms, models and reliability prediction," Microelectronics Reliability 39, no. 10, pp. 1445-1460, October 1999. DOI: https://doi.org/10.1016/S0026-2714(99)00051-7

[3] A. Ghetti (2004). Gate Oxide Reliability: Physical and Computational Models. In: Dabrowski, J., Weber, E.R. (eds) Predictive Simulation of Semiconductor Processing. Springer Series in MATERIALS SCIENCE, vol 72. Springer, Berlin, Heidelberg. https://doi.org/10.1007/978-3-662-09432-7_6.

[4] J. W. McPherson, "Time dependent dielectric breakdown physics – Models revisited," Microelectronics Reliability 52, pp. 1753-1760, 2012. DOI: http://dx.doi.org/10.1016/j.microrel.2012.06.007.

[5] R. Chau, S. Datta, M. Doczy, B. Doyle, J. Kavalieros, and M. Metz, "High-k/Metal–Gate Stack and Its MOSFET Characteristics," IEEE Electron Device Lett., vol. 25, pp. 408-410, June 2004. DOI: https://doi.org/10.1109/LED.2004.828570.

[6] H.-J. Lee, S. Rami, S. Ravikumar, V. Neeli, K. Phoa, B. Sell, and Y. Zhang, "Intel 22nm FinFET (22FFL) Process Technology for RF and mm Wave Applications and Circuit Design Optimization for FinFET Technology," 2018 IEEE International Electron Devices Meeting (IEDM), pp. 14.1.1-14.1.4, 2018. DOI: https://doi.org/10.1109/IEDM.2018.8614490.

[7] J. W. McPherson and H. C. Mogul, "Underlying physics of the thermochemical *E* model in describing low-field time-dependent

dielectric breakdown in SiO2 thin films," J. Appl. Phys., vol. 84, p. 1513, 1998. DOI: https://doi.org/10.1063/1.368217.

[8] J. W. McPherson, J. Y. Kim, A. Shanware, H. Mogul, "Termochemical description of dielectric breakdown in high dielectric constant materials", Appl. Phys. Lett., vol. 82, no. 13, pp. 2121-2123, 2003.

[9] J.W. McPherson, J. Kim, A. Shanware; H. Mogul, and J. Rodriguez, "Trends in the ultimate breakdown strength of high dielectric-constant materials," IEEE Transactions on Electron Devices 50, no 8, pp. 1771-1778, August 2003. DOI: https://doi.org/10.1109/TED.2003.815141.

[10] Ih-Chin Chen, S.E. Holland, and Chenming Hu, "Electrical breakdown in thin gate and tunneling oxides," IEEE Transactions on Electron Devices 32, no 2, pp. 413-422, February 1985. DOI: https://doi.org/10.1109/T-ED.1985.21957.

[11] Ih-Chin Chen, S.E. Holland, and Chenming Hu, "Hole trapping and breakdown in thin SiO2," IEEE Electron Device Lett., vol. 7, no. 3, pp. 164-167, March 1986. DOI: https://doi.org/10.1109/EDL.1986.26332.

[12] E. Miranda, J. Sune, R. Rodriguez, M. Nafria, and X. Aymerich, "A function-fit model for the soft breakdown failure mode," IEEE Electron Devices Letters, vol. 20, no. 6, pp. 265-267, June 1999. DOI: https://doi.org/10.1109/55.767093.

[13] E. Wu, A. Vayshenker, E. Novak, J. Sune R.-P. Vollersten, W. Lai, and D. Harmon, "Experimental evidence of TBD power-law for voltage dependence of oxide breakdown in ultrathin gate oxides," in IEDM Technical Digest, pp.541–544, 2000. DOI: https://doi.org/10.1109/IEDM.2000.904375.

[14] E. G. Liniger, S. A. Cohen, and G. Bonilla, "Low-field TDDB reliability data to enable accurate lifetime predictions," 2014 IEEE International Reliability Physics Symposium (IRPS), p. BD4.1, 2014. DOI: https://doi.org/10.1109/IRPS.2014.6861117.

[15] E. Y. Wu, and J. Sune, "Power-law voltage acceleration: A key element for ultra-thin gate oxide reliability," Microelectronics Reliability vol. 45, no. 12, pp. 1809-1834, Dec. 2005. DOI: https://doi.org/10.1016/j.microrel.2005.04.004.

[16] A.-M. El-Sayed, M. B. Watkins, A. L. Shluger, and V. V. Afanas'ev, "Identification of intrinsic electron trapping sites in bulk amorphous silica from ab initio calculations," Microelectronic Engineering 109, pp. 68-71, September 2013. DOI: https://doi.org/10.1016/j.mee.2013.03.027.

[17] D. Z. Gao, J. Strand, A.-M. El-Sayed, A. L. Shluger, A. Padovani, and L. Larcher, "Role of electron and hole trapping in the degradation and breakdown of SiO_2 and HfO_2 films," 2018 IEEE International Reliability Physics Symposium (IRPS), p. 5A.2-1, 2018. DOI: https://doi.org/10.1109/IRPS.2018.8353602.

[18] A. Padovani, D. Z. Gao, A. L. Shluger, L. Larcher, "A microscopic mechanisms of dielectric breakdown in SiO_2 films: an insight from multi-scale modeling," J. Appl. Phys., vol. 121, p. 155101, 2017. DOI: https://doi.org/10.1063/1.4979915.

[19] J. Strand, L. Larcher, A. Padovani, P. La Torraca, and A. L. Shluger, "Dielectric breakdown in HfO_2 dielectrics: using a multiscale modelling to identify the critical physical process involved in oxide degradation," J. Appl. Phys., vol. 131, p. 234501, 2022. DOI: https://doi.org/10.1063/5.0083189.

[20] Applied Materials Ginestra®. https://www.appliedmaterials.com/eu/en/semiconductor/ginestra-software.html

[21] D. Z. Gao, Al-M. El-Sayed and A. L. Shluger, "A mechanism for Frenkel defect creation in amorphous SiO_2 facilitated by electron injection", Nanotechnology, vol. 27, p. 505207, November 2016. DOI: https://doi.org/10.1088/0957-4484/27/50/505207.

[22] J. Strand, M. Kaviani, and A. L. Shluger, "Defect creation in amorphous HfO_2 facilitated by hole and electron injection", Microel. Eng. vol 178, p. 279-283, May 2017. http://dx.doi.org/10.1016/j.mee.2017.05.005.

[23] S. R. Bradley and A. L. Shluger, "Electron-Injection-Assisted Generation of Oxygen Vacancies in Monoclinic HfO_2", Phys. Rev. Applied, vol. 4, p. 064008, December 2015. DOI: https://doi.org/10.1103/PhysRevApplied.4.064008.

[24] D. Z. Gao, J. Strand, M. S. Munde, and A. L. Shluger, "Mechanisms of oxygen vacancy aggregation in SiO_2 and HfO_2", Frontiers in Physics, vol. 7, article 43, March 2019. DOI: https://doi.org/10.3389/fphy.2019.00043.

[25] J. W. Strand, J. Cottom, L. Larcher, and A. L. Shluger, "Effect of electric field on defect generation and migration in HfO2", Phys. Rev. B, vol. 102, p. 014106, July 2020. DOI: https://doi.org/10.1103/PhysRevB.102.014106.

[26] L. Vandelli, A. Padovani, L. Larcher, R.G. Southwick III, W.B. Knowlton, and G. Bersuker, "A physical model of the temperature dependence of the current through SiO2/HfO2 stacks," IEEE Trans. Electron Devices, vol. 58, no. 9, pp. 2878-2887, 2011. DOI: https://doi.org/10.1109/TED.2011.2158825.

[27] A. Padovani, L. Larcher, G. Bersuker, and P. Pavan, "Identifying the First Layer to Fail in Dual-Layer SiO_x/HfSiON Gate Dielectric Stacks" IEEE Electron Device Lett., vol. 34, no. 10, pp. 1289-1291, October 2013. DOI: https://doi.org/10.1109/LED.2013.2275182.

[28] P. La Torraca, F. M. Puglisi, A. Padovani, and L. Larcher, "Multiscale Modeling for Application-Oriented Optimization of Resistive Random-Access Memory," Materials, vol. 12, p. 3461, November 2019. DOI: https://doi.org/10.3390/ma12213461.

[29] A. Padovani, M. Pesic, F. Nardi, V. Milo, L. Larcher, M. A. Kumar, and Md Z. Baten, "Reliability of Non-Volatile Memory Devices for Neuromorphic Applications: A Modeling Perspective (Invited)," 2022 IEEE International Reliability Physics Symposium (IRPS), 2022. DOI: https://doi.org/10.1109/IRPS48227.2022.9764451.

[30] A. Padovani, B. Kaczer, M. Pešic, A. Belmonte, M. Popovici, L. Nyns, D. Linten, V. V. Afanas'ev, I. Shlyakhov, Y. Lee, H. Park, and L. Larcher, "A sensitivity map-based approach to profile defects in MIM capacitors From I–V, C–V, and G–V measurements," IEEE Transactions on Electron Devices, vol. 66, no. 4, pp. 1892–1898, April 2019. DOI: https://doi.org/10.1109/TED.2019.2900030.

[31] G. Jegert, A. Kersch, W. Weinreich, P. Lugli, „Monte Carlo Simulation of Leakage Currents in TiN/ZrO_2/TiN Capacitors," IEEE Transactions on Electron Devices, vol. 58, pp.327-334, 2011. DOI: https://doi.org/10.1109/TED.2010.2090158.

[32] K.A. Nasyrov, V.A. Gritsenko, "Charge transport in dielectrics via tunneling between traps," J. Appl. Phys., vol. 109, p. 093705, 2011. DOI: https://doi.org/10.1063/1.3587452.

[33] K. Huang, A. Rhys, "Theory of light absorption and non-radiative transition in F-centres" *Proc. R. Soc. London*, vol. 204A, pp. 406-423, 1950. DOI: https://doi.org/10.1098/rspa.1950.0184.

[34] C. H. Henry, D. V. Lang, "Non radiative capture and recombination by multiphonon emission in GaAs and GaP", Phys. Rev. B, vol. 15, no. 2, pp. 989-1016, 1977. DOI: https://doi.org/10.1103/PhysRevB.15.989.

[35] F. Jiménez-Molinos, A. Palma, F. Gámiz, J. Banqueri, and J. A. López-Villanueva, "Physical model for trap-assisted inelastic tunneling in metal-oxidesemiconductor structures," J. Appl. Phys., vol. 90, pp. 3396-3404, 2001. DOI: https://doi.org/10.1063/1.1398603.

[36] C. H. Henry, D. V. Lang, "Non radiative capture and recombination by multiphonon emission in GaAs and GaP", Phys. Rev. B, vol. 15, no. 2, pp. 989-1016, 1977. DOI: https://doi.org/10.1103/PhysRevB.15.989.

[37] L. Vandelli, A. Padovani, L. Larcher, and G. Bersuker, "Microscopic modeling of electrical stress-induced breakdown in poly-crystalline hafnium oxide dielectrics," IEEE Transactions on Electron Devices, vol. 60, no. 5, pp. 1754-1762, 2013. DOI: https://doi.org/10.1109/TED.2013.2255104.

[38] A. Padovani and L. Larcher, "Time-dependent dielectric breakdown statistics in SiO2 and HfO2 dielectrics: Insights from a multi-scale modeling approach," in IEEE International Reliability Physics Symposium Proceedings, 2018, vol. 1, pp. 86–93. DOI: https://doi.org/10.1109/IRPS.2018.8353552.

[39] A. Padovani, L. Larcher, G. Bersuker, and P. Pavan, "Charge transport and degradation in HfO2 and HfOx dielectrics," IEEE Electron Device Lett., vol. 34, no. 5, pp. 680–682, May 2013. doi: https://doi.org/10.1109/LED.2013.2251602.

[40] E. Wu, D. L. Harmon, and L.-K. Han, "Interrelationship of voltage and temperature dependence of oxide breakdown for ultrathin oxides," IEEE Electron Device Letters 21, no 7, July 2000. DOI: https://doi.org/10.1109/55.847381.

[41] E. Wu, J. Aitken, E. Novak, A. Vayshenker, P. Varekamp, G. Hueckel, and J. McKenna, "Voltage-Dependent Voltage-Acceleration of Oxide Breakdown for Ultra-Thin Oxides," IEEE Transactions on Electron Devices 49, no 12, pp. 2244-2253, December 2002. DOI: https://doi.org/10.1109/TED.2002.805606.